Dynamic Effects on Force Measurements. 2. Lubrication and the Atomic Force Microscope

ARTICLE *in* LANGMUIR · FEBRUARY 2003

Impact Factor: 4.46 · DOI: 10.1021/la026419f · Source: OAI

2 AUTHORS:

Olga I Vinogradova
Russian Academy of Sciences
111 PUBLICATIONS **3,390** CITATIONS
SEE PROFILE

Gleb Yakubov
University of Queensland
49 PUBLICATIONS **972** CITATIONS
SEE PROFILE

Dynamic Effects on Force Measurements. 2. Lubrication and the Atomic Force Microscope

Olga I. Vinogradova*,†,‡ and Gleb E. Yakubov†,‡

Max Planck Institute for Polymer Research, Postfach 3148, D-55021 Mainz, Germany, and Laboratory of Physical Chemistry of Modified Surfaces, Institute of Physical Chemistry, Russian Academy of Sciences, 31 Leninsky Prospect, 117915 Moscow, Russia

Received August 16, 2002. In Final Form: December 2, 2002

We present the results of investigations of high-speed drainage of a thin film confined between a microscopic colloidal probe and a substrate performed with a new atomic force microscope-related setup. Theoretical calculations are used to formulate the governing equation (force balance) for instantaneous deflection of a cantilever spring, which is due to both concentrated forces acting on a colloidal probe and viscous drag force on a cantilever itself. The suggested way to subtract the latter contribution allows design of a lubrication experiment. Two pairs of interacting solids, characterized by different wettability and smoothness, immersed into water−electrolyte solutions have been studied. Results for hydrophilic silica surfaces are in excellent agreement with the Reynolds theory of hydrodynamic lubrication. Faster drainage of a thin film confined between hydrophobic rough polystyrene surfaces is consistent with the theory of film drainage between slippery surfaces. The slip lengths are found to be of the order of the size of asperities, and do not depend on the separation and shear rate. The results are important for colloidal dynamics and nanofluidics.

I. Introduction

Recent years have seen an increase in the number of devices available to measure interaction forces between two surfaces separated by a thin film. Here we focus on the atomic force microscope (AFM), which was invented[1] to image the topography of surfaces but is now becoming an important tool for investigating surface interactions.[2] As in the original (static) version of the surface force apparatus (SFA),[3] in the AFM the force is obtained from the deflection of a measuring spring or cantilever. What is different from the SFA, where the cantilever deflection is detected interferometrically, is that the AFM uses electronic or digitally analyzed optical methods to sense it. Another difference is that various electronic techniques are used to control the motion of the surface. Besides that, the original AFM data, that is, the deflection versus the position of the piezo curves, are much more sensitive at high speed than the SFA separation versus time curves.[4] A corollary of all this is that the AFM is much more convenient than the SFA for force measurements at very high speed, that is, for studying the highly dynamic phenomena in a thin gap. Moreover, the AFM force measurements are always dynamic, because we always deal with dynamic thinning, or "drainage", of a liquid film confined between approaching surfaces, that is, a squeeze film geometry.[5] Therefore, special care should be taken to approach a quasi-static regime.[6] Despite these obvious advantages of the AFM design for studying thin film drainage, this technique has only rarely been used for high-speed lubrication (drainage) investigations.[7−9] In contrast to this, a number of SFA methods have been developed and successfully applied for this purpose.[4,10−16] The reason for such an apparent paradox is two complications connected with the use of the AFM at high speed. First are the "hardware" difficulties, which are mostly due to the creep and hysteresis of the oscillating piezo, its calibration, and position control. Second are what we call "software" complications, caused by difficulties in the interpretation of experimental data. On one hand, this is the direct consequence of the "hardware" problems that lead, for example, to the uncertainty in determining the zero in both separation and force. On the other hand, this reflects the AFM configuration geometry, where the typical size of a colloidal probe is much smaller than the size of the cantilever. The complication due to viscous "hysteresis" was already mentioned in the early reports.[17−19] In the previous paper[5] of this series we have calculated, both numerically and analytically, the contribution to the total deflection caused by a hydrodynamic drag on the cantilever, and we demonstrated that it is normally non-negligible.

This paper deals with the quantitative studying of thin film drainage with the AFM. First we generalize the asymptotic approach developed in ref 5 to the real situation

* Corresponding author. E-mail: vinograd@mpip-mainz.mpg.de.
† Max Planck Institute for Polymer Research.
‡ Russian Academy of Sciences.

(1) Binnig, G.; Quate, S. F.; Gerber, C. *Phys. Rev. Lett.* **1986**, *56*, 930.
(2) Ducker, W. A.; Senden, T. J.; Pashley, R. M. *Nature* **1991**, *353*, 239.
(3) Israelachvili, J. N.; Adams, G. E. *J. Chem. Soc., Faraday Trans. 1* **1978**, *74*, 975.
(4) Chan, D. Y. C.; Horn, R. G. *J. Chem. Phys.* **1985**, *83*, 5311.
(5) Vinogradova, O. I.; Butt, H. J.; Yakubov, G. E.; Feuillebois, F. *Rev. Sci. Instrum.* **2001**, *72*, 2330.
(6) Ishida, N.; Sakamoto, M.; Miyahara, M.; Higashitani, K. *J. Colloid Interface Sci.* **2001**, *235*, 190.
(7) Butt, H. J.; Döppenschmidt, A.; Hüttl, G.; Müller, E.; Vinogradova, O. I. *J. Chem. Phys.* **2000**, *113*, 1194.
(8) Craig, V. S. J.; Neto, C.; Williams, D. R. M. *Phys. Rev. Lett.* **2001**, *87*, 054504.
(9) Bonaccurso, E.; Kappl, M.; Butt, H. J. *Phys. Rev. Lett.* **2002**, *88*, 076101.
(10) Israelachvili, J. N. *J. Colloid Interface Sci.* **1986**, *110*, 263.
(11) Lodge, K. B.; Mason, R. *Proc. R. Soc. London, A* **1982**, *383*, 279.
(12) George, J. M.; Millot, S.; Loubet, J. L.; Tonck, A. *J. Chem. Phys.* **1993**, *98*, 7345.
(13) Horn, R. G.; Vinogradova, O. I.; Mackay, M. E.; Phan-Thien, N. *J. Chem. Phys.* **2000**, *112*, 6424.
(14) Vinogradova, O. I.; Horn, R. G. *Langmuir* **2001**, *17*, 1604.
(15) Zhu, Y.; Granick, S. *Phys. Rev. Lett.* **2001**, *87*, 096105.
(16) Baudry, J.; Charlaix, E.; Tonck, A.; Mazuyer, D. *Langmuir* **2001**, *17*, 5232.
(17) Hoh, J. H.; Engel, A. *Langmuir* **1993**, *9*, 3310.
(18) O'Shea, S. J.; Welland, M. E. *Langmuir* **1998**, *14*, 4186.
(19) Viani, M. B.; Schäffer, T. E.; Chand, A.; Rief, M.; Gaub, H. E.; Hansma, P. K. *J. Appl. Phys.* **1999**, *86*, 2258.

10.1021/la026419f CCC: $25.00
Published on Web 01/23/2003

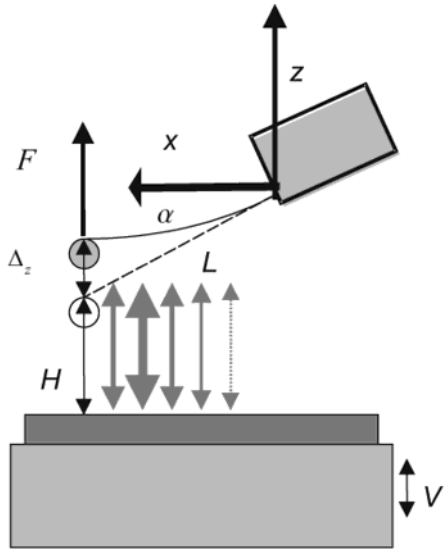

Figure 1. AFM cantilever deflected due to a concentrated force at one end and a nonuniform hydrodynamic pressure along the length of the cantilever.

of AFM force measurements, and we incorporate the deflection due to hydrodynamic pressure on the cantilever to the AFM force balance. One question of interest is how to subtract accurately the contribution of viscous drag on the cantilever to the total cantilever deflection. Another is how to analyze the remaining concentrated force acting on a colloidal probe. Second, we describe the dynamic force measurements with a new AFM-related setup, which is free from the usual AFM "hardware" problems. Third, we present the results of such measurements for two systems. As an initial application of the experimental technique and theoretical method, we have chosen to study silica and polystyrene surfaces immersed in aqueous electrolyte solutions. Extensions of our method to study other systems would be straightforward.

II. Theoretical Modeling

For the sake of brevity, only a condensed description of the theory and main ideas is given here. Some of the details are presented in Appendices.

A. Limiting Expressions for Deflection of the AFM Cantilever. First, we summarize and extend earlier relationships for the deflection of a tilted cantilever (as sketched in Figure 1) which are pertinent to the present analysis.[5] We consider a rectangular cantilever of width w and length L (assuming $\epsilon = w/L \ll 1$). In other words, we limit ourselves to asymptotic expressions, which can easily be handled.[20] However, here we do not apply the limitation of a small tilt angle, as done previously.[5] One reason is the relatively large tilt angle of the commercial setups (13° at the Nanoscope (Digital Instrumental) and 11° in the Molecular Force Probe (Asylum Research), for example). Another reason is that a large tilt angle can be used to minimize the contribution to the deflection from the viscous flow on the cantilever.

A Vertical Force at the End Only, No Drag on the Cantilever. The force F is negative for an attractive interaction and positive in the case of repulsion. If $(dz/dx)^2 \ll 1$, then the relation between the bending moment due to the elastic response of a cantilever and its curvature is described as

$$M = EI\frac{d^2z}{dx^2} \tag{1}$$

where I is the moment of inertia and E is Young's modulus.

The bending moment is also equal to a torque about the point at x, exerted by the applied force

$$M = F(L\cos\alpha - x) \tag{2}$$

where α is the tilt angle.

Combining eqs 1 and 2, we derive a differential equation for the shape of the cantilever

$$F(L\cos\alpha - x) = EI\frac{d^2z}{dx^2} \tag{3}$$

The boundary conditions express the fact that both position and slope are fixed at one end

$$z(0) = 0, \quad z'(0) = -\sin\alpha \tag{4}$$

This gives us the cantilever shape

$$\Delta_z^{(1)}(x) = z(x) + x\sin\alpha = \frac{F}{EI}\left(\frac{Lx^2\cos\alpha}{2} - \frac{x^3}{6}\right) \tag{5}$$

and the deflection due to a concentrated force at the end is given by

$$\Delta_z^{(1)}(L) = \frac{F}{2k}(-1 + 3\cos\alpha) \tag{6}$$

where $k = 3EI/L^3$ is the spring constant.

In the first-order approximation, the deflection of a cantilever due to a concentrated force at the end does not depend on the small tilt angle ($\alpha \to 0$), because in this case eq 6 is reduced to $\Delta_z^{(1)}(L) = F/k$, the equation which is normally used to relate a deflection to a force. An important point to note is that the use of this simplified equation does not really affect the results of equilibrium force measurements. Indeed, for a tilt angle of 11° (Molecular Force Probe) the force is underestimated only by 2.8%, and for a tilt angle of 13° (Nanoscope) it is only underestimated by 3.9%. This mistake can be treated as small.

A Distributed Normal Pressure Only. In the dynamic force experiment the cantilever width and the gap between a cantilever and substrate could be of the same order, which could lead to a complicated description of the flow. However, approximate expressions for the drag force can nevertheless be written, as was suggested previously for two spheres,[22] by simply adding the drag force calculated from Stokes flow on an isolated body and Reynolds flow

(20) We clarify our point of view by using the simplest case of a rectangular cantilever. In reality, the cantilevers are often V-shaped. The parallel beam approximation[40] is commonly used as a model of V-shaped AFM cantilevers in analytical evaluations of the spring constant. Such a model, being applied to the calculation of the hydrodynamic behavior of the cantilever, would lead to the very cumbersome calculations. One can, however, use another approach, based on the fact that the only combination having the dimension of a force is μvD, where D is some characteristic size of the body. This means that for a thin gap the drag force can be expressed as $F \sim \mu vD \times \text{function}(D/H, D'/H)$, where D' is some characteristic size. One can, therefore, suggest that the deflection of a real V-shaped cantilever will be determined by the equations derived in this paper, provided that L is still the cantilever length but w is some appropriately chosen effective width. An important point to note is that for the V-shaped cantilevers the approximation of a narrow cantilever will often not be valid. Therefore, the use of such cantilevers would require a more complicated numerical approach.[5]

(21) Neto, C.; Craig, V. S. J. *Langmuir* **2001**, *17*, 2097.

(22) Barnocky, G.; Davis, R. H. *J. Colloid Interface Sci.* **1988**, *121*, 226.

for a thin gap. By its definition, the first force gives a deflection which is independent of the gap.

Here we first focus on the lubrication (Reynolds) flow. In the lubrication approximation, the Navier−Stokes equation gives

$$\nabla_t p \sim \mu \frac{\partial^2 v_t}{\partial z^2} \tag{7}$$

where $v_t = \{v_x; v_y\}$ is the tangential component of the fluid velocity and $\nabla_t = \{\partial/\partial x; \partial/\partial y\}$. In this notation, the continuity equation is

$$\frac{\partial v_z}{\partial z} + \nabla_t v_t = 0 \tag{8}$$

where v_z is the normal component of the velocity field. We have to solve the system of differential equations (eqs 7 and 8) with the boundary conditions

$$\text{At } z = -x \sin\alpha + \Delta_z^{(2)}: \qquad v_z = \dot{\Delta}_z^{(2)}, \quad v_t = 0$$

$$\text{At } z = -(L \sin\alpha + H): \qquad v_z = -\dot{H} = -v, \quad v_t = 0$$

with the deflection $\Delta_z^{(2)} = \Delta_z^{(2)}(x, t)$. Here $H(t)$ is the minimum gap between substrate and a cantilever. We further assume $\Delta_z^{(2)} > 0$ and $v < 0$ for a substrate moving in the z direction.

The assumption $\epsilon \ll 1$ and estimates of the orders of magnitude allow further simplification ($\nabla_t \sim \partial/\partial y$) to be made to give an analytical solution of eqs 7 and 8. Taking into account that $p = 0$ at both $y = 0$ and $y = w$, we derive

$$p = \frac{6\mu y(y - w)(v + \dot{\Delta}_z^{(2)})}{D^3} \tag{9}$$

where

$$D = D(x, t) = H + \sin\alpha(L - x) + \Delta_z^{(2)} \tag{10}$$

is the gap between the substrate and a deflected cantilever. In eq 10 one can safely omit $\Delta_z^{(2)}$. This can be justified provided the deflection is small, that is, when $\Delta_z^{(2)} \ll H + \sin\alpha(L - x)$. This is the typical experimental situation, because the deflection of the cantilever is usually less than 200 nm, while the minimum possible separation $H \sim 2R$, where $2R = 3-10\ \mu$m is the typical diameter of the attached sphere. In fact, in some resent experiments even larger spheres were used.[8,9,21] Therefore, the bending moment is expressed as

$$M(x, t) = \int_0^w \int_x^L p(x', y)(x' - x)\, dy\, dx' = -\mu w^3 \left[\frac{v}{2 \sin\alpha}\left(\frac{1}{H^2} - \frac{1}{(H + (L - x)\sin\alpha)^2}\right) + \int_x^L \frac{\dot{\Delta}_z^{(2)}(x, t)\, dx}{(H + (L - x)\sin\alpha)^3}\right] \tag{11}$$

The final integro-differential equation for a cantilever shape $\Delta(x, t)$ is

$$\frac{\partial^2 \Delta_z^{(2)}}{\partial x^2} = \frac{3M}{kL^3} \tag{12}$$

with the boundary conditions

$$\Delta_z^{(2)}(0, t) = 0, \quad \frac{\partial \Delta_z^{(2)}(0, t)}{\partial x} = 0, \quad \frac{\partial \Delta_z^{(2)}(0, t)}{\partial t} = 0 \tag{13}$$

The governing equations for cantilever shape can be further simplified if the velocity of deflection $\dot{\Delta}_z^{(2)}$ is small compared with the speed of piezo v (In previous work[5] we have also made such an assumption). This limitation leads to an analytical solution for the deflection of the cantilever end:

$$\Delta_z^{(2)}(L) = z(L) + \sin\alpha L = -\frac{3v\mu L}{8k}\left(\frac{w}{H}\right)^3 \gamma_1^* \tag{14}$$

with

$$\gamma_1^* = \frac{4\gamma}{3}\left[1 - \frac{3\gamma}{2} + 3\gamma^2 - 3\gamma^3 \ln\left(1 + \frac{1}{\gamma}\right)\right] \tag{15}$$

where $\gamma = H/(L \sin\alpha)$. The dimensionless function γ_1^* has been interpreted as a correction for tilt angle between the surfaces in the expression for the deflection of a narrow horizontal cantilever. It follows from eq 14 that the viscous drag on the cantilever cannot change as strongly with distance as H^{-3}. However, this limiting case can be expected only when $\gamma \gg 1$. Taking into account that H/L is always $\ll 1$, this asymptotic form is easily violated even for very small α. Hence, in contrast to the deflection due to a concentrated force at the end of the cantilever, the deflection due to the distributed hydrodynamic pressure is sensitive to the tilt angle α even when it is small.

The approximation is justified (see Appendix A) provided that

$$\dot{\Delta}_z^{(2)}/v \sim -\frac{3v\mu}{8k \sin\alpha}\left(\frac{w}{H}\right)^3 \ll 1$$

This inequality is valid in the typical AFM force dynamic experiment.

The deflection due to Stokes flow could be presented as

$$\dot{\Delta}_z^{(3)} \sim -\frac{3v\mu LA}{8k}$$

In this expression A is a fitting parameter which depends on the cantilever geometry.

B. Force Balance. The AFM force balance should incorporate both the (concentrated) force on the sphere and the drag on the cantilever.

Assuming $\Delta_z = \Delta_z^{(1)} + \Delta_z^{(2)} + \Delta_z^{(3)}$, the force balance corresponding to the dynamic force measurements can be written as

$$\Delta_z = \frac{F}{2k}(-1 + 3\cos\alpha) - \frac{3v\mu L}{8k}\left[\left(\frac{w}{H}\right)^3 \gamma_1^* + A\right] \tag{16}$$

C. Concentrated Forces Acting on the Sphere. The forces acting on the sphere may be treated as concentrated in the scale of our problem. In the dynamic AFM experiment these are hydrodynamic and surface forces, that is

$$F = F_h + F_s \tag{17}$$

The hydrodynamic force can be written as[22]

$$F_h = -6\mu\pi R \frac{dh}{dt}\left(1 + \frac{R}{h} f^*\right) \tag{18}$$

where h is the distance between the sphere and substrate,

and f^* is the correction for deviations from the Reynolds flow in the thin gap.

Equation 18 is in agreement with the lubrication force[24] for $h/R \ll 1$ and with the Stokes drag for $h/R \gg 1$.

We stress that the hydrodynamic drag on a sphere is proportional to the velocity of the relative motion. In the case of a bare cantilever, this was approximately equal to that of the moving substrate v. For an attached sphere, this simplification is no longer valid, and in the general case, the velocity of a sphere relative to the substrate $dh/dt \neq v$.

One reason for deviations from Reynolds theory could be liquid slippage over a solid surface (for a review see ref 23). The expressions for correction for slippage in the case of surfaces with different, but constant, slip lengths are given in Appendix B.

D. Summary. To finish this section, the deflection of a cantilever in a dynamic force experiment in the general case reflects both a colloidal probe−substrate interaction and a cantilever−substrate interaction. We have formulated the equations of motion (force balance) that take both these effects into account and allow design of a lubrication experiment. The important thing to stress is that the contributions from different terms to the force balance have different functional dependences on the main experimental parameters. Therefore, they can be separated/subtracted independently on their absolute value and/or their ration. Below we present experimental data that support our theoretical predictions.

III. Experimental Section

The experimental setup was similar to that described in refs 26−28. Cantilevers were fixed in a holder with $\alpha \sim 5-20°$. To measure the drainage curves, the cuvette was moved vertically toward the cantilever with a 12 μm range piezoelectric translator (Physik Instrumente, Germany). This translator is equipped with integrated capacitance position sensors, which provide measurements of their actual position and further adjustment of piezo movement. This feature leads to an accuracy of 0.005%, which means that for piezo travel of 12 μm the maximum error is 0.6 nm. During the movement the deflection of the cantilever was measured with an optical lever technique. For this, the light of a laser diode (3 mW, 670 nm) was focused onto the back of the gold coated cantilever using microfocusing optics (spot diameter is about 8 μm), and after reflection from the cantilever and from another mirror the position of the reflected laser spot was measured with a two-dimensional position sensitive detector (PSD) (SiTek, Sweden, active area 2×2 cm^2). Drainage curves were measured in the time range from 20 s to 250 ms per force curve. This corresponds to driving speeds from 1 to 20 μm/s. To calculate speed of piezo movement in the case of a triangular drive function, we simply multiply piezo oscillation frequency by double the piezo range distance. To convert the output voltage of the position sensitive device to a deflection in nanometers, we calculate the slope of the constant compliance line of the force curve, where any change in height position is equal to the change in deflection. The result of a force measurement is a plot of the cantilever deflection Δ_z versus the height position of the piezo translator.

We use rectangular tipless cantilevers covered with 3 nm of chromium and 40 nm of gold ($w = 52$ μm and $L = 450$ μm, which gives $\epsilon = 0.12$). The spring constant ($k \sim 0.1-0.2$ N/m) of the cantilever was determined by the method of power spectrum density of the cantilever thermal noise described in ref 29. To decrease the hydrodynamic drag of the liquid on the cantilever and in order to vary R and H independently, we have designed a "snowman" probe (Figure 2). To fabricate "snowman" probes, glass spheres (Duke Scientific, Palo Alto, CA) of 10 μm radius were attached on the top of the cantilever using epoxy glue and then clean silica or polystyrene particles (both from Bangs Labs, Fisher, IN) were attached approximately on the top of the glass spheres using epoxy glue or a sintering method. Spheres were glued with UV-curing Norland optical adhesive No. 81 (Norland Products, New Brunswick, NJ). After spheres were attached on the cantilevers, they were exposed for 10 min under UV irradiation (12 W, $\lambda = 254$ nm) until complete adhesive solidification. This glue is resistive to most organic solvents, including tetrahydrofuran (Aldrich, Germany) and toluene, which means the lowest level of contamination connected with the glue. After formation of the "snowman", probes were cleaned in an oxygen plasma for 5 min. Immediately after cleaning, probes were mounted in the setup and immersed in the experimental cuvette. After 10−30 min, cantilever drift normally disappeared and measurements were performed. The geometric parameters of experiments for further analysis were obtained from analysis of scanning electron microscope (SEM) microphotographs, as shown in Figure 3.

The first pair of interacting surfaces studied was a silica or a borosilicate glass sphere (Bangs Labs Inc., Carmel, USA) with average radius 1.85 and 5.2 μm (prepared and attached to a cantilever as described above) against a silicon wafer cleaned with the same procedure. All surfaces were considered to be hydrophilic and are found to be molecularly smooth. Root-mean-square roughness over a 1 μm × 1 μm area was in the range 0.3

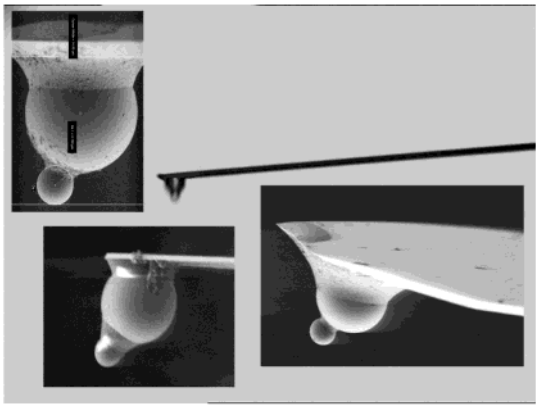

Figure 2. Video microscope image of an AFM cantilever with the attached colloidal "snowman" probe. The insets show scanning electron microscope images for various glued and sintered "snowmen".

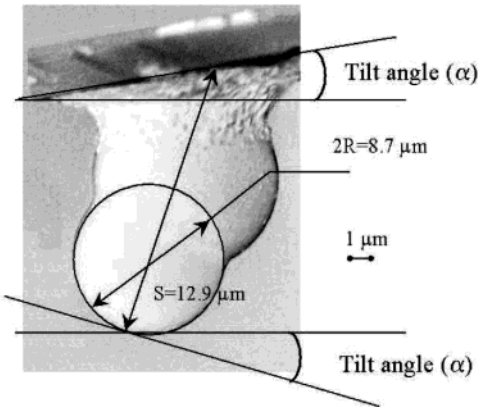

Figure 3. Example of the geometric parameters of the experiment determined from scanning electron microscope images. S denotes the "snowman height"

(23) Vinogradova, O. I. *Int. J. Miner. Process.* **1999**, *56*, 31.
(24) Vinogradova, O. I. *Langmuir* **1995**, *11*, 2213.
(25) Vinogradova, O. I.; Feuillebois, F. *J. Colloid Interface Sci.* **2000**, *221*, 1.
(26) Yakubov, G. E.; Butt, H. J.; Vinogradova, O. I. *J. Phys. Chem. B* **2000**, *104*, 3407.
(27) Vinogradova, O. I.; Yakubov, G. E.; Butt, H. J. *J. Chem. Phys.* **2001**, *114*, 8124.
(28) Ecke, S.; Raiteri, R.; Bonaccurso, E.; Reiner, C.; Deiseroth, H. J.; Butt, H. J. *Rev. Sci. Instrum.* **2001**, *72*, 4164.
(29) Hutter, J. L.; Bechhöfer, J. *Rev. Sci. Instrum.* **1993**, *64*, 1868.

nm for both an individual sphere and a wafer. No indications of larger asperities or peaks were detected. We treat these surfaces as smooth, because their roughness is of the order of the accuracy of the determination of surface separation. We also consider them to be hydrophilic, because the measurements of the contact angle on the silicon water, done by observation of a sessile drop with a commercial setup (Data Physics, Germany), showed complete wetting.[30]

The second pair of interacting surfaces was a polystyrene latex sphere (Bangs Labs Inc., Carmel, USA) of radius 4.38 μm against a polystyrene plate. The preparation of polystyrene surfaces was done as before.[27,31] Imaging of the polystyrene plate with a regular AFM tip revealed that it is as smooth as the silica surfaces. The polystyrene spheres were found to be significantly rougher, and the root-mean-square roughness over a 1 μm × 1 μm area was in the range 2.2−2.8 nm. The maximum peak-to-valley height difference was found to be 15 nm. We therefore treat these spheres as rough. Measurements of the contact angle on the planar polystyrene surface have given a receding contact angle of 86°. The advancing angle is found to be 92°. The contact angle of polystyrene microspheres was determined with a procedure described earlier.[31,32] The contact angles measured with different polystyrene particles varied by ±4° from particle to particle. The average receding contact angle was 68°, and the average advancing contact angle was −92°, that is, the same as that for a polystyrene plate.

Experiments were carried out in 10^{-1} M (polystyrene) and 10^{-3} M (glass and silica) NaCl (99.99%, Aldrich) aqueous solutions. Water for solutions was prepared using a commercial Milli-Q system containing ion-exchange and charcoal stages.

IV. Results

The original deflection versus distance curves for a typical force experiment performed at different speeds are shown in Figure 4 (top). The zero deflection (force) position was determined by invoking symmetry of the hydrodynamic force acting on the system (cantilever and sphere) at large separation during approach and retraction. Surface forces acting on the sphere are, in the general case, negligibly small at separations larger than 1 μm. In our case, they can be ignored at distances above 20 nm. Therefore, the zero-deflection position corresponds to the middle line of the long-range part of the drainage curve. One can see that the absolute value of deflection increases with the approaching velocity and decreases with the separation. This confirms that the total deflection measured in the experiment contains a hydrodynamic contribution. The large range of measured deflection suggests that the drag on a cantilever plays an important role.

A. Viscous Drag on a Cantilever. We now start with the analysis of data for the deflection of the cantilever at long-range distances due to nonuniform hydrodynamic pressure. Measurements presented in Figure 4 (bottom) test the approximate expressions (eq 14) for the deflection due to drag on a cantilever. Here we illustrate our approach by using a relatively small tilt angle (α is roughly 4°) in order to have a larger contribution to deflection due to flow around the cantilever. The results of several series of measurements are also presented in the scaled form. The scaling is chosen according to eq 14. The results from several experiments suggest that the measurements are in perfect agreement with the theoretical predictions and that for all the experiments (with this particular configuration geometry) the Stokes drag can be described by taking $A = 36$. Therefore, in the subsections below we present and analyze only the concentrated force acting on the sphere obtained by subtracting the deflection of the cantilever from the total deflection measured. The error we introduce with such a procedure is mostly due to uncertainty in the measurement of the tilt angle (±1°).

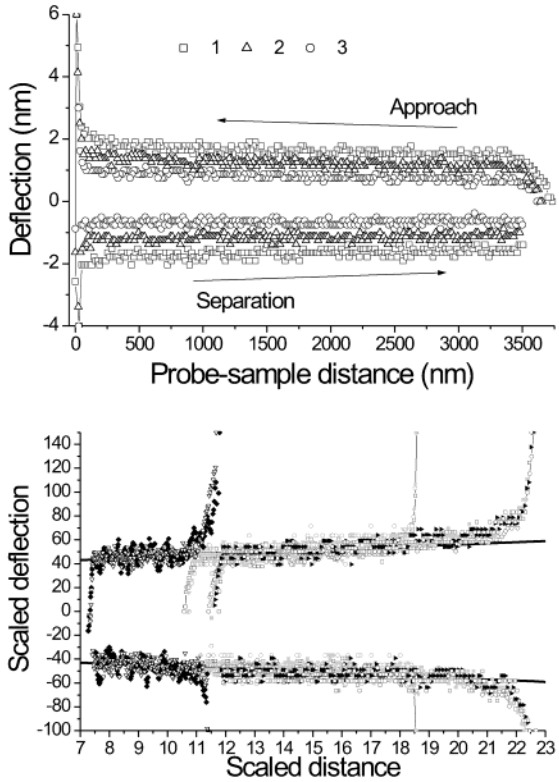

Figure 4. Total cantilever deflection in the dynamic AFM force experiment ($\alpha = 5.0 \pm 0.5°$). (top) Original data obtained at the driving speeds ±20 μm/s (1), ±15 μm/s (2), and ±10 μm/s (3). The experiment was performed with a 1.9 μm snowman probe ("snowman height" is 14.0 μm). (bottom) Set of different measurements presented in the scaled form: scaled deflection is $-8\Delta_z/(3k\nu\mu L)$; scaled distance is $\gamma_1^*(w/H)^3$. Approach speed varied from −6 to −20 μm/s; the "snowman heights" and sphere radii were from 10.4 μm to 15.2 μm, and from 1.9 μm to 5.4 μm, correspondingly. The straight line has the slope "1" ("−1" for the retraction part of the curve). The negative and positive "peaks" correspond to the regions close to the initial distance and contact. These regions have been excluded from the analysis of a flow on cantilever, because here its deflection is not solely due to a drag force on it.

B. Interaction of Smooth Hydrophilic Silica and Glass Surfaces. The aim of this subsection is to demonstrate that one can make a quantitative analysis of the concentrated force acting on a sphere. As a first step, the procedure includes the DLVO fit for simple simple silica and glass systems at low speed. One question of interest is, "When can the AFM force measurements be treated as a quasiequilibrium?" In other words, "Which speed can be considered to be slow enough to avoid a dynamic contribution to the deflection versus position curve?" It follows from our results that a speed below 1 μm/s can normally be treated as slow. There is no speed dependence of the total deflection at v below 1 μm/s, but a higher speed of a piezo translator gives different results for different speeds, which indicates a contribution from hydrodynamic drag. At low speed the force is exponentially decaying with a decay length equal to the Debye length for our electrolyte solution (in all these experiments we used 10^{-3} M solutions). The parameters of this double layer repulsion F_s have been obtained from measurements at speed 0.1 μm/s for every given pair of interacting surfaces. We also remark that these quasi static force measurements have

(30) Unfortunately, to our knowledge, there is no routine way of making contact angle measurements on hydrophilic microspheres.

(31) Yakubov, G. E.; Vinogradova, O. I.; Butt, H. J. *Colloid J.* **2001**, *63*, 518.

(32) Yakubov, G. E.; Vinogradova, O. I.; Butt, H. J. *J. Adhesion Sci. Technol.* **2001**, *14*, 1783.

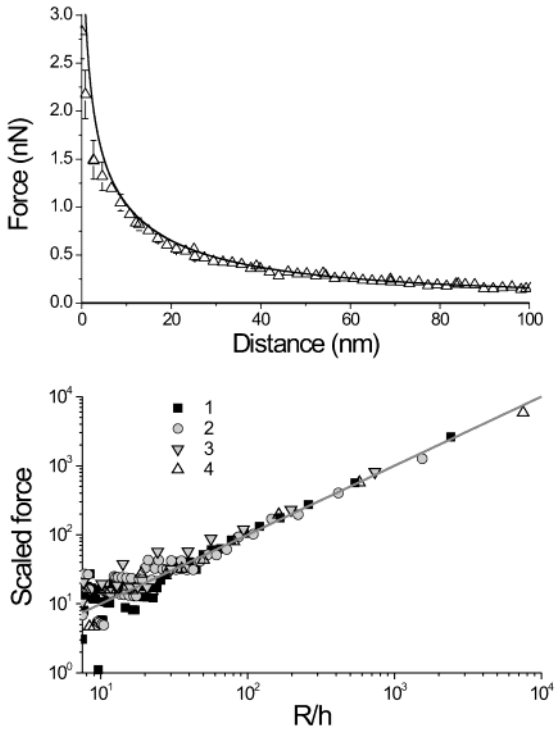

Figure 5. Hydrodynamic force acting on the hydrophilic spheres. (top) Original force vs distance data obtained with a 5.2 μm probe at the driving speed -20 μm/s (triangles), and a theoretical curve obtained by numerical solution of the force balance equation (solid curve). (bottom) Scaled hydrodynamic force $-F_h/(6\pi\mu\ dh/dt) - 1$ plotted against R/h. Driving speed was -20 μm/s (curves 1 and 3) and -10 μm/s (curves 2 and 4); cantilever sample distances (1, 2$-$10.4 μm; 3, 4$-$14.0 μm); sphere's radii (1, 2$-$5.2 μm; 3, 4$-$1.9 μm). The slope of the solid line is equal to $f^* = 1$.

revealed neither any hysteresis between approach and retraction data nor an adhesion peak.

Figure 5 shows the original drainage data obtained at different driving speeds and a scaled hydrodynamic force. Two ways have been used to analyze the hydrodynamic force. The first algorithm was similar to that used previously in the SFA experiment[4,13] and included a numerical solution of the differential equation (eq 17) for a concentrated force to fit the experimental data. In this procedure we used the experimentally measured values of R, h, k, A, and parameters of the double layer force, obtained from low-speed measurements. Then, performing the least-squares fit of data for a concentrated force, we obtain the slip lengths b_1 and b_2 for interacting surfaces. The second algorithm was based on subtracting the double layer force from the total force acting on the sphere and on a subsequent analysis of F_h, by assuming it is described by eq 18. This analysis included a calculation of f^* for a given h, and a least-squares fit of this correction for slippage to get b_1 and b_2. It was found that both approaches lead to the same results. The main conclusion made from the inspection of experimental data (see Figure 5) is that no slippage ($b_1 = b_2 = 0 \pm 1$ nm) is observed within the experimental accuracy. The important point to note is that the large sphere of the "snowman" configuration does not implicate our results. Rough estimates of the possible contribution of such a sphere are given in Appendix C. The substitution of typical experimental values to eq 20 suggests that the contribution from the large "snowman" sphere never exceeds 5% of the drag acting on the small sphere in the lubrication regime. This is confirmed by the fact that the same results (i.e. no slip) are obtained both for a silica sphere of radius 1.85 μm of the "snowman" probe and for a borosilicate glass sphere of radius 5.2 μm attached to a cantilever. Our experiment, therefore, does not confirm the recent statement,[9] made for a similar system (borosilicate sphere of $R = 10$ μm against a silicone wafer), that the smooth hydrophilic surface is characterized by a rate dependent slip length of the order of 10 nm. Unfortunately, we cannot comment more about the reasons for such a discrepancy, because a lot of the details of analysis are omitted in that publication.

Table 1. Contribution from Different Terms to the Deflection of a Cantilever in a Typical High-Speed Experiment (Borosilicate Glass Sphere of $R = 5.2$ μm)[a]

h, nm	Δ_z, nm	$\Delta_z^{(1)}$, nm		$\Delta_z^{(2)} + \Delta_z^{(3)}$, nm
		$v = 20$ μm/s		
3000	2.3			2.3
1000	2.7		0.1	2.6
100	3.8		1.0	2.8
20	8.1	1.3	3.9	2.9
5	17.2	6.2	8.2	2.9
		$v = 1$ μm/s		
3000	0.1			0.1
1000	0.1			0.1
100	0.2		0.1	0.1
20	1.6	1.3	0.2	0.1
5	6.8	6.1	0.5	0.1

[a] In the column for $\Delta_z^{(1)}$ the numbers on the left correspond to a contribution from a surface force, and the numbers on the right to a contribution from a hydrodynamic force.

In summary, our results for smooth hydrophilic surfaces are in excellent agreement with the Reynolds theory of hydrodynamic lubrication with no-slip boundary conditions. It would be useful to those interested in measuring hydrodynamic forces to have some feeling about the relative contribution of different terms to the total deflection described by eq 16. We are now in a position to estimate it. Table 1 illustrates how important the different terms could be depending on the driving speed and separation. One can see that, for the high speed experiment, the contribution due to the cantilever is indeed significant and has to be subtracted by using our model and a large distance fit, as suggested here. At low speed the contribution from flow on a cantilever can safely be ignored, and the deflection is mostly due to colloidal forces. However, even at such a speed there could be some contribution from the hydrodynamic force on the sphere acting at separations of a few nanometers.

C. Interaction of Rough Hydrophobic Polystyrene Surfaces. The quasi-equilibrium colloidal interactions between hydrophobic polystyrene surfaces have been studied before.[27,35] It was found that two types of interaction in such a system are possible. One is observed only in dilute solutions and is of electrostatic origin.[27] Another[27,35] is characterized by an abrupt long-range jump of the surfaces into contact due to formation of nanobubbles[36−39] at the rough hydrophobic surface of polystyrene spheres. Here we focus only on the drainage behavior of

(33) Vinogradova, O. I. *Langmuir* **1998**, *14*, 2827.
(34) Vinogradova, O. I. *Langmuir* **1996**, *12*, 5963.
(35) Considine, R. F.; Hayes, R. A.; Horn, R. G. *Langmuir* **1999**, *15*, 1657.
(36) Vinogradova, O. I.; Bunkin, N. F.; Churaev, N. V.; Kiseleva, O. A.; Lobeyev, A. V.; Ninham, B. W. *J. Colloid Interface Sci.* **1995**, *173*, 443.
(37) Bunkin, N. F.; Lobeyev, A. V.; Movchan, T. G.; Ninham, B. W.; Vinogradova, O. I. *Langmuir* **1997**, *13*, 3024.
(38) Ishida, N.; Inoue, T.; Miyahara, N.; Higashitani, K. *Langmuir* **2000**, *16*, 6377.
(39) Tyrell, J. W. G.; Attard, P. *Langmuir* **2002**, *18*, 160.
(40) Sader, J. E. *Rev. Sci. Instrum.* **1995**, *66*, 4583.

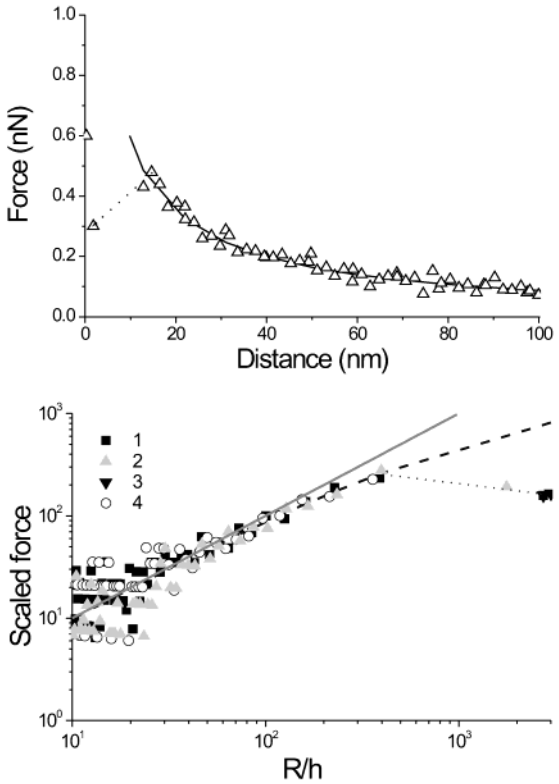

Figure 6. Hydrodynamic force acting between hydrophobic polystyrene surfaces. (top) Original force vs distance data obtained with a 4.9 μm probe (triangles) (driving speed -20 μm/s) against a polystyrene surface. The solid curve corresponds to the theoretical calculations for symmetric cases with slip length 4 nm. The dotted arrow shows jump into a contact. (bottom) Scaled concentrated hydrodynamic force [$F_h/(6\pi\mu\, dh/dt) - 1$] acting on the hydrophobic polystyrene spheres plotted against R/h. Driving speed was -20 μm/s (curves 1 and 3) and -10 μm/s (2); "snowman heights" were 13.3 μm (1, 2) and 12.4 μm (3); small sphere radii were 4.9 μm (1, 2), 4.4 μm (3), and 1.9 μm (4). The solid line corresponds to the no-slip case. The dashed line corresponds to a slip case with the slip length 4 nm. The dotted arrow shows jump into a contact.

this system, where the attractive surface interaction is mediated by nanobubbles. Due to complicated analysis of double layer forces in such a system, we here use only 10^{-1} M solution and are therefore in the situation when the double layer forces are of much shorter range and weaker than hydrodynamic drag.

Figure 6 presents the results obtained in several series of measurements. Presentation of the results in scaled form clearly demonstrates that drainage is faster than that for the hydrophilic case even before the jump into contact. The analysis of data was performed in a way similar to what we used in the previous subsection. The best fit was provided when the values of the slip lengths were constant and confined between the pairs $b_1 = 10 \pm 1$ nm against $b_2 = 0.5 \pm 1$ nm, and $b_1 = b_2 = 4 \pm 1$ nm. In other words, the drainage of a thin film confined between hydrophobic rough polystyrene surfaces is in agreement with the theory of film drainage between slippery surfaces,[24] and the slip lengths are of the order of the size of asperities. Whether this is a consequence of roughness itself, or nanobubble formation on a rough hydrophobic surface, remains an open question which will be studied in future publications. Our current approach does not allow us to draw any further conclusions about the origin of slippage in polystyrene systems.

Acknowledgment. We thank François Feuillebois for helpful suggestions that led to Appendix A, and Gunnar Glasser for making SEM images.

Appendix A: Assumption of Small Deflection Velocity

The assumption that led to eq 14 is that the deflection velocity is small as compared with v, or $\dot{\Delta}_z^{(2)} v \ll 1$. We will now check under which experimental conditions this is indeed true and if this condition is equivalent to a condition of a small deflection, which is always valid.

Taking the time derivative of $\Delta_z^{(2)}$, we find

$$\frac{\dot{\Delta}_z^{(2)}}{v} = -\frac{3\mu v w^3 \Gamma}{8kL^3 \sin^4 \alpha}$$

with

$$\Gamma = -\frac{2}{3}\frac{\gamma + 4 - 3\gamma^2 - 6\gamma^3}{\gamma^3(\gamma + 1)} - 4\ln\left(1 + \frac{1}{\gamma}\right)$$

One can show that $\Gamma \times \gamma^3 = O(1)$ for realistic values of γ. Therefore,

$$\frac{\dot{\Delta}_z^{(2)}}{v} \sim -\frac{3v\mu}{8k \sin \alpha}\left(\frac{w}{H}\right)^3$$

Using typical numerical values of experiment, we get $\dot{\Delta}_z^{(2)}/v \sim 10^{-4}$; that is, the deflection velocity is indeed small.

Appendix B: Correction for Slippage in the Equations for a Viscous Drag on a Sphere

In the case of surfaces with different, but constant, slip lengths $b_1 = b = \beta h$ and $b_2 = b(K + 1) = \beta h(K + 1)$, where K can have values between -1 and ∞, it takes the form[24,25]

(i) $K \to -1$

$$f^* = \frac{1}{4}\left(1 + 3\cdot 2\cdot \frac{1}{4\beta}\left[\left(1 + \frac{1}{4\beta}\right)\ln(1 + 4\beta) - 1\right]\right)$$

(ii) $K \to \infty$

$$f^* = \frac{1}{4}\cdot 2\cdot \frac{1}{3\beta}\left[\left(1 + \frac{1}{3\beta}\right)\ln(1 + 3\beta) - 1\right]$$

(iii) $K \neq -1$, $K \neq \infty$

$$f^* = -\frac{2x_1}{\beta x_2 x_3} - \frac{2}{\beta^2(x_3 - x_2)}\left[\frac{(\beta x_2 + 1)(x_2 - x_1)}{x_2^2}\ln(1 + \beta x_2) - \frac{(\beta x_3 + 1)(x_3 - x_1)}{x_3^2}\ln(1 + \beta x_3)\right] \quad \text{(B1)}$$

with

$$x_1 = 2 + K$$

$$x_2 = 2(2 + K + \sqrt{1 + K + K^2})$$

$$x_3 = 2(2 + K - \sqrt{1 + K + K^2})$$

We note that, due to a misprint, the factor 2 in the first term of case iii was lost in ref 24 (and corrected in ref 25). This, however, did not affect the limiting expression for

$K \to 0$ derived in ref 24 and intensively used during the last few years.[9,13,15,16]

Appendix C: Estimate of the Hydrodynamic Interaction between the Large Sphere of the "Snowman" and Substrate

The presence of the large "snowman" sphere of radius R_2 can contribute to the deflection of the cantilever, because this sphere can interact hydrodynamically with the substrate. Determination of the exact amount of this hydrodynamic interaction would require a complicated three-dimensional Stokes flow problem. We can nevertheless give an estimate of this effect by using the simplified approach suggested in ref 5. The main assumption is that at $r \le R_1$ the flow is blocked by the small sphere of radius R_1, but at $r > R_2$ the flow is not affected by the attached sphere.

The standard consideration (see, for example, ref 34) leads to the following differential equation for pressure p

$$\frac{\mathrm{d}}{\mathrm{d}r}\left(H^3 r \frac{\mathrm{d}p}{\mathrm{d}r}\right) = 12\mu v r$$

where $H = h + r^2/2R_2$. Then the assumption $\mathrm{d}p/\mathrm{d}r = 0$ at $r = R_1$ leads to

$$p = \frac{3\mu v R_2}{H^2} + \frac{3\mu v {R_1}^2}{h^3}\left[\frac{h^2}{2H^2} + \ln\left(1 - \frac{h}{H}\right) + \frac{h}{H}\right]$$

The expression for a force is given by

$$F_\mathrm{h} = 2\pi R_2 \int_{h_1}^{\infty} p \, \mathrm{d}H$$

where $h_1 = h + {R_1}^2/2R_2$. The integration gives

$$F_\mathrm{h} = \frac{6\pi\mu v {R_2}^2}{h}\left(1 + A_1 A_2\left[\frac{A_1 A_2}{2}\ln\left(1 + \frac{2}{A_1 A_2}\right) - 1\right]\right) \quad \text{(C1)}$$

with $A_1 = R_1/R_2 < 1$ and $A_2 = R_1/h = R_1/(h^* + 2R_1) \sim {}^1/_2$. If $A_1 \ll 1$, the equation for a force can be further simplify and give

$$F_\mathrm{h} \sim \frac{3\mu\pi v {R_2}^2}{R_1}\left(1 - \frac{R_1}{2R_2}\right)$$

LA026419F